Research Square

Preprints are preliminary reports that have not undergone peer review.
They should not be considered conclusive, used to inform clinical practice,
or referenced by the media as validated information.

A one-dimensional Cd(II) coordination polymer based on 2,5- dibromobenzene-1,4-dicarboxylate: Crystal structure and dielectric properties

Bakhtiyor Chori ugli Tursunov
Institute of General and Inorganic Chemistry of Uzbekistan Academy of Sciences
Yakubov Yuldash Yusupbaevich
Institute of General and Inorganic Chemistry of Uzbekistan Academy of Sciences
Khayit Khudaynazarovich Turaev
Termez State University
A. Aditya Prasad
adityaaraveti@gmail.com

CMR Technical Campus
Abrorbek Khamidjanovich Ruzmetov
Institute of Bioorganic Chemistry Uzbekistan Academy of Sciences
Adkhamjon Sadullayevich Normamatov
Institute of Bioorganic Chemistry Uzbekistan Academy of Sciences
Avazbek Bakhtiyarovich Ibragimov
Institute of Bioorganic Chemistry Uzbekistan Academy of Sciences
Lutfulla Bozorov
Termiz State Pedagogical Institute
Sadridin Eshkaraev
Termez University of Economics and Service
Aziz Bakhtiyarovich Ibragimov
Institute of General and Inorganic Chemistry of Uzbekistan Academy of Sciences
Balakrishnan Chellakarungu
Institute of General and Inorganic Chemistry of Uzbekistan Academy of Sciences

---

Research Article

Keywords: Cadmium(II) coordination polymer, Crystal structure, Hirshfeld surface analysis, Dielectric properties, Charge transport

Posted Date: August 27th, 2026

DOI: https://doi.org/10.21203/rs.3.rs-10694267/v1

License: This work is licensed under a Creative Commons Attribution 4.0 International License.
Read Full License

Additional Declarations: No competing interests reported.

Version of Record: A version of this preprint was published at Journal of Materials Science: Materials in Electronics on October 26th, 2026. See the published version at https://doi.org/10.1007/s10854-026-18718-3.

Abstract

A new one-dimensional cadmium(II) coordination polymer, $[Cd(Br_2\text{-}BDC)(2\text{-}MeIm)_2(DMF)]_n$, was synthesized under solvothermal conditions and comprehensively characterized by single-crystal X-ray diffraction, spectroscopic, microscopic, thermal, dielectric, and electrical techniques. Single-crystal X-ray diffraction revealed that the compound crystallizes in the monoclinic space group $P2_1/n$, in which seven-coordinate Cd(II) centres are bridged by μ_2-2,5-dibromobenzene-1,4-dicarboxylate ligands to form an infinite one-dimensional coordination polymer. Continuous shape-measure analysis established a distorted pentagonal-bipyramidal CdN_2O_5 coordination geometry, while N–H···O and C–H···O hydrogen-bonding interactions further consolidate the crystal structure into a three-dimensional supramolecular network. Hirshfeld surface analysis showed that H···H, C···H/H···C, O···H/H···O, and Br···H/H···Br contacts dominate the intermolecular interactions. FT–IR and Raman spectroscopy confirmed the coordination modes of the Br_2-BDC, 2-methylimidazole, and DMF ligands, whereas SEM–EDS analysis verified the plate-like morphology and elemental composition of the coordination polymer. Thermal analysis demonstrated multistep decomposition with structural stability up to approximately 180°C. Dielectric measurements revealed frequency- and temperature-dependent polarization characterized by decreasing dielectric constant and dielectric loss with increasing frequency, while AC conductivity followed a thermally activated hopping-type charge-transport mechanism. The correlation between the one-dimensional coordination architecture and the dielectric response demonstrates that $[Cd(Br_2\text{-}BDC)(2\text{-}MeIm)_2(DMF)]_n$ is a promising coordination polymer for dielectric and frequency-dependent electronic applications.

1. Introduction

Metal–organic frameworks (MOFs) and coordination polymers (CPs) represent one of the most rapidly expanding fields of modern coordination chemistry owing to their remarkable structural diversity and wide range of potential applications in gas storage and separation, catalysis, sensing, luminescence, magnetism, electronics, and energy-related technologies [1, 2]. The rational design of such materials relies on the judicious selection of metal ions and multifunctional organic ligands capable of generating predictable architectures with tailored dimensionality, topology, and physicochemical properties. Advances in crystal engineering have enabled the construction of sophisticated coordination frameworks ranging from discrete molecular assemblies to multidimensional porous networks, thereby providing opportunities for the development of advanced functional materials [3, 4].

Among the numerous organic ligands employed in coordination chemistry, aromatic polycarboxylates have attracted considerable attention because of their versatile coordination behaviour and strong affinity toward metal ions. Their rigid aromatic backbones and multiple oxygen-donor sites enable the formation of structurally robust coordination frameworks with diverse topologies. Furthermore, aromatic dicarboxylates frequently participate in hydrogen-bonding and π–π stacking interactions that contribute significantly to crystal stabilization and supramolecular organization [5, 6]. Functionalized terephthalate

derivatives are particularly attractive because substituents on the aromatic ring can modify framework geometry, crystal packing, pore environment, and physicochemical properties. Among these ligands, 2,5-dibromobenzene-1,4-dicarboxylic acid (H_2Br_2BDC) has emerged as an effective building block for constructing structurally diverse coordination polymers and MOFs. The presence of bromine substituents introduces additional steric and electronic effects that frequently influence coordination modes, intermolecular interactions, framework stability, and adsorption behaviour. Previous investigations have demonstrated that Br_2BDC can support the formation of one-, two-, and three-dimensional architectures with transition-metal, alkaline-earth, and lanthanide ions, resulting in materials exhibiting interesting luminescent, adsorption, and sensing properties [7, 8]. Mixed-ligand Zn(II) and Co(II) coordination polymers containing Br_2BDC and bipyridyl ligands have revealed notable structural diversity and photoluminescent behaviour, highlighting the important role of auxiliary ligands in directing framework assembly [9, 10].

Nitrogen-donor heterocyclic ligands are frequently introduced into coordination systems to enhance structural complexity and provide additional coordination sites. Imidazole derivatives are particularly attractive because of their strong metal-binding ability, structural rigidity, and ability to participate in hydrogen-bonding interactions [11]. Such ligands often act as structure-directing agents that influence framework dimensionality, connectivity, and stability. Among them, 2-methyl-1H-imidazole (2-MeIm) has proven to be an effective auxiliary ligand capable of stabilizing metal centres while promoting the formation of extended coordination architectures. The combination of O-donor carboxylates and N-donor imidazole ligands, therefore, represents an efficient strategy for constructing mixed-ligand coordination polymers with enhanced structural diversity and tunable physicochemical properties [12, 13].

The structural chemistry of cadmium(II) is especially attractive for the design of coordination polymers. Owing to its relatively large ionic radius, flexible coordination geometries, and d^{10} electronic configuration, Cd(II) can accommodate a wide variety of ligand environments and generate coordination compounds with diverse structural motifs. As a consequence, cadmium-based coordination polymers display rich structural diversity, including discrete molecular complexes, one-dimensional chains, layered architectures, and three-dimensional frameworks [14, 15]. Moreover, Cd(II)-containing materials often exhibit interesting luminescent, adsorption, sensing, and electrical properties, making them attractive candidates for multifunctional materials research [8]. Solvent molecules frequently play a significant role in coordination framework assembly. N,N-Dimethylformamide (DMF), one of the most widely used solvents in solvothermal synthesis, often acts not only as a reaction medium but also as a coordinating ligand. Coordinated DMF molecules may occupy vacant coordination sites, stabilize metal centres, influence crystal growth, and affect framework geometry through secondary interactions. Consequently, DMF-assisted coordination frequently contributes to the formation of structurally unique architectures with enhanced stability and well-defined coordination environments [16, 17].

Despite the considerable progress in the development of Br_2BDC-based coordination materials, systems that simultaneously incorporate Cd(II) ions, Br_2BDC ligands, 2-methyl-1H-imidazole, and coordinated

DMF molecules remain relatively uncommon [18]. Furthermore, most reported studies have focused primarily on crystal structures, topology, thermal stability, luminescence, and adsorption behaviour, whereas dielectric and electrical transport properties have received comparatively little attention. Recently, increasing interest has been devoted to the dielectric characteristics and A.C. conductivity behaviour of coordination polymers because these properties provide valuable information regarding polarization mechanisms, dielectric relaxation processes, and charge-carrier transport phenomena in crystalline materials. Such investigations are essential for understanding structure–property relationships and evaluating the potential of coordination frameworks for electronic and dielectric applications [19, 20].

In the present work, we report the synthesis and comprehensive characterization of a new one-dimensional cadmium(II) coordination polymer, *catena-poly*[[bis(2-methyl-1H-imidazole-κN)(N,N-dimethylformamide-κO)cadmium(II)]-(μ_2-2,5-dibromobenzene-1,4-dicarboxylato-κ^2O:O′)], hereafter abbreviated as $[Cd(Br_2BDC)(2\text{-MeIm})_2(DMF)]_n$ (Br_2BDC = 2,5-dibromobenzene-1,4-dicarboxylate; 2-MeIm = 2-methyl-1H-imidazole; DMF = N,N-dimethylformamide). The compound was synthesized under solvothermal conditions and structurally elucidated by single-crystal X-ray diffraction. The one-dimensional chain structure is generated through μ_2-Br_2BDC bridges connecting neighbouring Cd(II) centres, while two terminal 2-MeIm ligands and one coordinated DMF molecule complete the coordination environment around the metal centre. In addition, the structural features and physicochemical properties of the compound were systematically investigated by FT-IR spectroscopy, thermal analysis, dielectric measurements, and frequency-dependent A.C. conductivity studies. Particular attention was devoted to understanding the influence of the mixed O/N-donor ligand system on framework formation and elucidating the relationship among crystal structure, dielectric relaxation behaviour, and charge-transport mechanisms. These results provide new insight into brominated cadmium-based coordination polymers and contribute to the development of multifunctional coordination materials with potential dielectric and electronic applications.

2. Experimental

2.1. Synthesis of $[Cd(Br_2\text{-}BDC)_2(2\text{-}MeIm)_2(DMF)]_n$

All reagents and solvents were of analytical grade and used as received without further purification. $Cd(CH_3COO)_2{\cdot}4H_2O$ (0.3026 g, 1 mmol), 2,5-dibromoterephthalic acid (H_2Br_2BDC, 0.324 g, 1 mmol), and 2-methylimidazole (2-MeIm, 0.164 g, 2 mmol) were dissolved in a mixed solvent composed of distilled water (10 mL) and N,N-dimethylformamide (DMF, 5 mL) under continuous magnetic stirring at room temperature until a homogeneous solution was obtained. The resulting solution was transferred into a 15 mL Teflon-lined stainless-steel autoclave, sealed, and heated at 150°C for 24 h under autogenous pressure. After completion of the reaction, the autoclave was allowed to cool gradually to room temperature at a rate of approximately 5°C h^{-1}. The resulting crystalline product was collected by filtration, washed thoroughly with distilled water and DMF to remove residual reactants, and dried in air

at room temperature. Colourless hexagonal crystals suitable for single-crystal X-ray diffraction analysis were obtained in 75% yield.

2.2. Characterization techniques

The synthesized coordination polymer, $[Cd(Br_2\text{-}BDC)(2\text{-}MeIm)_2(DMF)]_n$, was comprehensively characterized by spectroscopic, crystallographic, microscopic, thermal, and electrical techniques. FT–IR (Bruker) and Raman (Renishaw inVia, 300–3500 cm^{-1}) spectroscopy were employed to confirm ligand coordination and metal–ligand interactions. Surface morphology and elemental composition were investigated by SEM–EDS (JEOL JSM-IT210), while bulk elemental analysis was performed using XRF (PANalytical Epsilon-4). Thermal stability was evaluated by TG–DTA (Shimadzu DTG-60) under an argon atmosphere from room temperature to 800°C at a heating rate of 10°C min^{-1}. Single-crystal X-ray diffraction data were collected at 298 K on an Oxford Diffraction Xcalibur-R CCD diffractometer using Cu Kα radiation. The structure was solved with SHELXT, refined using SHELXL within Olex2, and analysed using CrystalExplorer, Mercury, and continuous shape-measure calculations. Dielectric properties, including the dielectric constant (ε'), dielectric loss (tan δ), and AC conductivity (σ_{ac}), were measured as functions of frequency and temperature to investigate polarization, dielectric relaxation, and charge-transport behaviour.

3. Results and Discussion

3.1. Single-crystal XRD analysis

3.1.1. Crystal structure description

The crystal structure of $[Cd(Br_2\text{-}BDC)(2\text{-}MeIm)_2(DMF)]_n$ was determined by single-crystal X-ray diffraction, and the crystallographic data are summarized in Table 1. The compound crystallizes in the monoclinic crystal system with the centrosymmetric space group $P2_1/n$. Structure refinement converged satisfactorily with low residual factors (R_1 = 0.0374 and wR_2 = 0.0906), confirming the high quality and reliability of the structural model. The refined structure exhibits negligible residual electron density, indicating an accurate description of the crystal architecture.

The ORTEP representation of the asymmetric unit is shown in Fig. 1(a). The asymmetric unit comprises one crystallographically independent Cd(II) ion, one μ_2-2,5-dibromobenzene-1,4-dicarboxylate ($Br_2\text{-}BDC^{2-}$) ligand, two terminal 2-methylimidazole (2-MeIm) ligands, and one coordinated *N,N*-dimethylformamide (DMF) molecule, corresponding to the empirical formula $C_{19}H_{21}Br_2CdN_5O_5$. The Br_2-BDC ligand bridges adjacent Cd(II) centres through its carboxylate groups, producing an infinite one-dimensional coordination polymer, while the 2-MeIm and DMF molecules occupy terminal coordination sites around the metal centre (Fig. 1(b)). The rigid aromatic backbone of the Br_2-BDC ligand serves as an efficient spacer between neighbouring Cd(II) ions, directing the propagation of the polymeric chain along the crystallographic direction.

Table 1
Crystal data and structure refinement for $[Cd(Br_2\text{-}BDC)(2\text{-}MeIm)_2(DMF)]_n$.

CCDC	**2564892**
Formula	$C_{19}H_{21}Br_2CdN_5O_5$
Formula Weight	671.62
Temperature (K)	293(2)
Wavelength	1.54184
Crystal System	monoclinic
Space group	$P2_1/n$ (No.14)
a, b, c [Å]	9.4303(2) 17.0011(3) 15.2670(4)
α, β, γ [°]	90 104.280(2) 90
V [$Å^3$]	2372.06(9)
Z	8
D(calc) [g/cm^3]	1.881
Mu(CuKα) [/mm]	11.665
F(000)	1312
Crystal Size [mm]	0.05x 0.30x 0.30
Theta range for data collection	3.96 to 67.70
Index ranges	$-6 \le h \le 11, -21 \le k \le 16, -19 \le l \le 18$
Reflections collected	15612
Independent reflections	4269
Absorption correction	multi-scan
Data/restraints/parameters	4286/34/294
Goodness-of-fit on F^2	1.0293
Final R indices [I>2sigma(I)]	$R_1 = 0.0374$, $wR_2 = 0.0906$
R indices (all data)	$R_1 = 0.0446$, $wR_2 = 0.0947$
Extinction coefficient	0.00055(6)
Largest diff. peak and hole ($e.Å^{-3}$)	0.840 and − 0.7144

Selected structural parameters (Table S1) reveal nearly equivalent C–O bond distances for both coordinated carboxylate groups [1.242(5)–1.263(5) Å], indicating significant resonance delocalization within the carboxylate moieties. The aromatic framework remains essentially planar, with C–Br bond lengths of 1.898(4) and 1.901(4) Å, confirming that bromine substitution does not appreciably disturb the ligand geometry. Likewise, the coordinated 2-methylimidazole ligands preserve their aromatic character, while the DMF molecule coordinates through its carbonyl oxygen atom with an O5–C19 bond length of 1.191(7) Å. These structural features demonstrate that coordination occurs without significant distortion of the ligand frameworks and provide a stable mixed O,N-donor environment around the Cd(II) centre.

3.1.2. Coordination environment and polymeric architecture

The coordination environment around the Cd(II) centre is illustrated in the polyhedral representation shown in Fig. 2. The metal ion adopts a seven-coordinate CdN_2O_5 environment, consisting of five oxygen atoms and two nitrogen atoms. Four oxygen atoms originate from two μ_2-Br_2-BDC^{2-} ligands, one oxygen atom is supplied by a coordinated DMF molecule, and the remaining two coordination sites are occupied by nitrogen atoms from independent 2-methylimidazole ligands. This mixed O,N-donor coordination sphere is typical of Cd(II), which readily accommodates higher coordination numbers because of its relatively large ionic radius. The Br_2-BDC ligand acts simultaneously as a chelating and bridging linker. Each ligand coordinates through both carboxylate groups to connect adjacent Cd(II) centres, thereby extending the structure into an infinite one-dimensional coordination polymer. In contrast, the two 2-methylimidazole ligands and the DMF molecule function as terminal ligands, completing the coordination sphere around the metal centre and contributing to the stabilization of the polymeric framework.

Table 2
Polyhedral parameters for $[Cd(Br_2\text{-}BDC)(2\text{-}MeIm)_2(DMF)]_n$

Bond	Distance(Å)
Cd(1)-N(1)	2.252(4)
Cd(1)-O(1)	2.531(5)
Cd(1)-O(5)	2.474(4)
Cd(1)-O(3)	2.621(4)
Cd(1)-O(4)	2.313(4)
Cd(1)-O(2)	2.385(4)
Cd(1)-N(3)	2.314(4)
Average bond length	2.4129
Polyhedral volume $Å^3$	20.7488
Distortion index (bond length)	0.04583
Effective coordination number	**6.2032**

Selected bond distances and bond angles are summarized in Tables 2 and S1. The Cd–donor bond distances span 2.252(4)–2.621(4) Å, with the shortest distance observed for Cd1–N1 [2.252(4) Å] and the longest for Cd1–O3 [2.621(4) Å]. The remaining Cd–O and Cd–N distances fall within the expected range for seven-coordinate Cd(II) complexes containing mixed oxygen- and nitrogen-donor ligands. The variation in bond lengths reflects the different donor abilities of the ligands and the geometric constraints imposed by the chelating carboxylate groups. The coordination sphere is further characterized by a wide distribution of bond angles. The smallest angles, O3–Cd1–O4 = 52.40(10)° and O1–Cd1–O2 = 52.88(9)°, arise from the bite angles of the chelating carboxylate groups, whereas the largest angle, O5–Cd1–N3 = 170.26(14)°, corresponds to an approximately trans arrangement between the coordinated DMF oxygen atom and the nitrogen atom of one 2-methylimidazole ligand. These geometric features indicate that the coordination environment deviates from an ideal seven-coordinate geometry owing to the combined influence of chelating and bridging ligands, together with the steric requirements of the terminal ligands.

3.1.3. Crystal packing and solvent-accessible surface

The crystal packing diagrams viewed along the *bc*, *ac*, and *ab* crystallographic planes (Fig. S1) reveal the regular arrangement of the one-dimensional coordination chains throughout the crystal lattice. The μ_2-Br_2-BDC ligands serve as rigid spacers between neighbouring Cd(II) centres, while the terminal 2-methylimidazole and coordinated DMF molecules are oriented around the polymeric backbone, resulting in efficient packing of the coordination chains. The absence of extended channels suggests a densely

packed framework with limited free volume. The topology-coloured solvent-accessible surface generated using Mercury with a probe radius of 1.2 Å (Fig. 3) further illustrates the packing characteristics of the structure. Small, isolated accessible voids are distributed throughout the crystal lattice; however, they remain discontinuous and do not form interconnected porous channels. The restricted solvent-accessible volume results from the close packing of the coordination chains together with the steric influence of the bromine substituents and terminal ligands. Consequently, the framework exhibits a compact architecture with limited internal void space, which contributes to its structural stability.

3.1.4. Polyhedral distortion and continuous shape measure analysis

A quantitative assessment of the coordination geometry was performed using polyhedral distortion parameters and continuous shape measure (CShM) calculations, and the results are summarized in Tables 2 and 3. The CdN_2O_5 coordination polyhedron possesses an average Cd–donor bond length of 2.4129 Å and a calculated polyhedral volume of 20.7488 $Å^3$, consistent with the relatively spacious coordination environment expected for seven-coordinate Cd(II). The calculated bond-length distortion index (DI = 0.04583) indicates a moderate deviation from ideal geometry arising from the mixed O,N-donor coordination environment. The effective coordination number (ECoN = 6.2032) is lower than the formal coordination number of seven, indicating that the donor atoms contribute unequally to the coordination sphere because of differences in Cd–ligand bond lengths.

Table 3
Calculated continuous shape measure values $[Cd(Br_2\text{-}BDC)(2\text{-}MeIm)_2(DMF)]_n$

[ML7]	HP-7	HPY-7	PBPY-7	COC-7	CTPR-7	JPBPY-7	JETPY-7
Cd(1)	32.505	21.070	**2.703**	8.350	6.744	6.399	20.211

The CShM calculations provide a quantitative comparison of the experimental coordination polyhedron with ideal seven-coordinate geometries. Among the models examined, the pentagonal bipyramid (PBPY-7) exhibits the lowest CShM value (2.703), whereas substantially larger values are obtained for the heptagon, hexagonal pyramid, capped octahedron, capped trigonal prism, Johnson pentagonal bipyramid, and Johnson elongated triangular pyramid. These results demonstrate that the CdN_2O_5 coordination environment is best described as a moderately distorted pentagonal bipyramid, consistent with the observed bond distances and angular distortions.

3.1.5. Predicted crystal morphology

The theoretical crystal morphology predicted using the Bravais–Friedel–Donnay–Harker (BFDH) method implemented in Mercury is shown in Fig. 4. The calculated crystal habit is characterized by a well-developed polyhedral morphology dominated by the (020), (0–20), (011), and (0–11) faces, together with several additional low-index crystallographic planes. The prominence of these faces reflects their relatively slow growth rates predicted by the BFDH model. The anisotropic crystal habit is closely related

to the one-dimensional coordination framework generated by the μ_2-Br_2-BDC ligands. The rigid aromatic backbone directs crystal growth along preferred crystallographic directions, whereas the coordinated 2-methylimidazole and DMF molecules influence the relative development of individual crystal faces through steric effects. Although the BFDH model does not consider solvent effects or surface energies, the predicted morphology provides a reasonable approximation of the external crystal habit based on crystallographic symmetry and lattice geometry.

3.1.6. Hydrogen-bonding interactions

The hydrogen-bonding interactions responsible for consolidating the crystal structure are summarized in Table 4. The supramolecular assembly is primarily stabilized by two strong intermolecular N–H···O hydrogen bonds involving the amino groups of the coordinated 2-methylimidazole ligands and the carboxylate oxygen atoms of neighbouring Br_2-BDC ligands. The N(2)–H(2)···O(2) and N(4)–H(4)···O(3) interactions exhibit donor–acceptor distances of 2.873(5) and 2.825(5) Å, respectively, with nearly linear bond angles of 169.2(6)° and 169.5(4)°, indicative of strong and highly directional hydrogen bonding. These interactions effectively connect adjacent coordination chains and reinforce the crystal packing. A weaker C(18)–H(18B)···O(5) interaction is also observed between the methyl group of a coordinated 2-methylimidazole ligand and the oxygen atom of the coordinated DMF molecule. The H···O distance of 2.43(3) Å, donor–acceptor separation of 2.793(10) Å, and bond angle of 102(2)° are characteristic of a weak C–H···O contact. Although considerably weaker than the N–H···O hydrogen bonds, this interaction provides additional stabilization to the molecular arrangement. Together, these hydrogen-bonding interactions reinforce the crystal packing and contribute to the structural stability of the one-dimensional coordination polymer.

Table 4
Hydrogen bonds for $[Cd(Br_2\text{-BDC})(2\text{-MeIm})_2(DMF)]_n$ [Å and °].

D-H•••A	d(D-H)	d(H•••A)	d(D•••A)	<(DHA)
N(2)-H(2)•••O(2)	0.860(5)	2.023(5)	2.873(5)	169.2(6)
N(4)-H(4)•••O(3)	0.860(6)	1.974(5)	2.825(5)	169.5(4)
C(18)-H(18B)•••O(5)	0.96(3)	2.43(3)	2.793(10)	102(2)

3.2. Hirshfeld surface analysis

To gain further insight into the intermolecular interactions governing the crystal packing of $[Cd(Br_2\text{-BDC})(2\text{-MeIm})_2(DMF)]_n$, a Hirshfeld surface analysis was performed using CrystalExplorer. The Hirshfeld surfaces mapped over d_e, d_i, d_{norm}, and fragment patch are shown in Fig. S2, while the corresponding two-dimensional fingerprint plots and percentage contributions of the intermolecular contacts are presented in Fig. 5 and Fig. S3, respectively. The d_{norm} surface exhibits several intense red regions corresponding to close intermolecular contacts that are shorter than the sum of the van der Waals radii [21]. These contacts are mainly associated with the strong N–H···O hydrogen bonds formed between the

amino groups of the coordinated 2-methylimidazole ligands and the carboxylate oxygen atoms of the Br_2-BDC ligands. Additional weaker red regions are attributable to C–H···O interactions involving the coordinated DMF molecules. The abundance of these red spots indicates that hydrogen bonding plays an important role in stabilizing the crystal structure. The surfaces mapped over d_e and d_i provide information about the external and internal intermolecular contacts, respectively, whereas the fragment patch surface highlights the contributions of neighbouring molecular fragments to the crystal packing and illustrates the distribution of intermolecular interactions around the coordination polymer [22].

The two-dimensional fingerprint plots quantitatively describe the contributions of various intermolecular contacts to the Hirshfeld surface. The largest contribution arises from H···H contacts (37.1%), reflecting the significant role of van der Waals interactions in the crystal packing. The second largest contribution is provided by C···H/H···C contacts (19.1%), which are associated with interactions between hydrogen atoms and the aromatic rings of the Br_2-BDC ligands. O···H/H···O interactions contribute 15.0% and appear as characteristic sharp spikes in the fingerprint plots, confirming the presence of strong and directional hydrogen-bonding interactions throughout the structure. Br···H/H···Br contacts account for 12.6%, indicating that bromine atoms also participate significantly in intermolecular contacts that influence the crystal packing. Smaller contributions originate from C···C contacts (5.6%), N···H/H···N contacts (4.3%), Br···O/O···Br contacts (2.9%), Br···C/C···Br contacts (1.3%), and Br···N/N···Br contacts (1.1%). Minor contributions from Br···Br contacts (0.6%), N···C/C···N contacts (0.3%), and O···C/C···O contacts (0.1%) are also observed. Although these interactions contribute only a small fraction of the total Hirshfeld surface, they collectively participate in the stabilization of the crystal packing. The Hirshfeld surface analysis indicates that the crystal packing of $[Cd(Br_2\text{-BDC})(2\text{-MeIm})_2(DMF)]_n$ is primarily governed by H···H van der Waals interactions, supported by C···H/H···C, O···H/H···O, and Br···H/H···Br contacts. These interactions cooperate to generate a stable three-dimensional supramolecular architecture, consistent with the structural features revealed by the single-crystal X-ray diffraction analysis [23].

3.3. Infrared spectral analysis.

The FT–IR spectrum of $[Cd(Br_2\text{-BDC})(2\text{-MeIm})_2(DMF)]_n$ exhibits characteristic absorption bands arising from the Br_2-BDC ligands, coordinated 2-MeIm molecules, coordinated DMF molecules, and Cd–ligand coordination bonds (Fig. S4). An absorption band centred at 3175 cm^{-1} is attributed to the N–H stretching vibrations of the coordinated 2-MeIm ligands. Weak bands observed at 3087 and 3032 cm^{-1} are assigned to aromatic C–H stretching vibrations of the imidazole and benzene rings [24]. Additional absorptions at 2963 and 2917 cm^{-1} correspond to aliphatic C–H stretching vibrations of the methyl groups present in the 2-MeIm and DMF molecules. A strong absorption band at 1666 cm^{-1} is assigned to the C = O stretching vibration of the coordinated DMF molecule, indicating coordination through the carbonyl oxygen atom to the Cd(II) centre. The coordinated Br_2-BDC ligand exhibits characteristic carboxylate stretching vibrations at 1560 and 1395 cm^{-1}, corresponding to the asymmetric $\nu_{as}(COO^-)$ and symmetric $\nu_s(COO^-)$ stretching modes, respectively. The separation between these bands ($\Delta\nu$ = 165

cm^{-1}) is consistent with the coordination of the carboxylate groups to the Cd(II) centre. These assignments are in good agreement with the single-crystal X-ray structure, which confirms the coordination of the DMF carbonyl oxygen atom and the carboxylate oxygen atoms of the Br_2-BDC ligand. The absorptions at 1289 and 1157 cm^{-1} are assigned to C–N and C–O stretching vibrations of the coordinated 2-MeIm and DMF ligands. Strong bands observed at 1108, 1053, and 1009 cm^{-1} arise from ring stretching and C–O vibrational modes of the organic ligands. These bands confirm the presence of both N-donor and O-donor ligands within the coordination framework [25]. Additional bands at 896, 841, and 786 cm^{-1} are associated with aromatic C–H out-of-plane bending vibrations of the dibromoterephthalate ligand. The absorptions at 744, 671, and 616 cm^{-1} are attributed to C–Br stretching vibrations and ring deformation modes of the Br_2-BDC ligand. The low-frequency absorptions at 535 and 479 cm^{-1} are assigned to Cd–O and Cd–N stretching vibrations together with lattice deformation modes, confirming the coordination of the carboxylate oxygen atoms, imidazole nitrogen atoms, and DMF oxygen atoms to the Cd(II) centres and the formation of the extended coordination polymer framework

3.4. Raman spectral analysis

The Raman spectrum of $[Cd(Br_2\text{-}BDC)(2\text{-}MeIm)_2(DMF)]_n$, recorded over the range 3500–300 cm^{-1}, is presented in Fig. S5. The spectrum exhibits well-defined vibrational bands arising from the coordinated Br_2-BDC, 2-MeIm, and DMF ligands, providing complementary evidence for the formation of the coordination polymer. The weak bands observed at 3081 and 2960 cm^{-1} are assigned to the aromatic and aliphatic C–H stretching vibrations of the Br_2-BDC, 2-MeIm, and DMF ligands. A weak feature at 1832 cm^{-1} is attributed to overtone or combination vibrational modes of the coordinated organic ligands. The strong bands at 1681 and 1626 cm^{-1} are assigned to the stretching vibrations of the coordinated carbonyl group of the DMF molecule and the coordinated carboxylate groups of the Br_2-BDC ligand, respectively, while the intense band at 1603 cm^{-1} corresponds to the aromatic C = C stretching vibration of the dibromoterephthalate ligand [26]. The prominent band at 1306 cm^{-1} is attributed to C–N stretching coupled with ring vibrational modes of the coordinated 2-methylimidazole ligand. The bands at 1262 and 1212 cm^{-1} are assigned to C–O stretching and in-plane deformation modes of the coordinated carboxylate and DMF ligands. The intense Raman band at 1071 cm^{-1} is assigned to the symmetric stretching vibration of the coordinated carboxylate groups coupled with aromatic ring vibrations of the Br_2-BDC ligand. The strong band at 876 cm^{-1} corresponds to aromatic C–H out-of-plane bending vibrations of the substituted benzene ring, whereas the weak band at 709 cm^{-1} is attributed to ring deformation modes of the aromatic framework. The low-frequency region contains characteristic vibrations associated with the metal–ligand bonds and the brominated aromatic ligand. The intense band at 348 cm^{-1} is assigned to the Cd–O stretching vibration, arising from the coordination of the carboxylate oxygen atoms of the Br_2-BDC ligand and the carbonyl oxygen atom of the coordinated DMF molecule. The band at 506 cm^{-1} is attributed to the Cd–N stretching vibration involving the coordinated 2-MeIm ligands, although a minor contribution from ligand skeletal deformation cannot be excluded. The

bands at 556, 596, and 632 cm^{-1} are assigned predominantly to C–Br stretching and skeletal deformation modes of the Br_2-BDC ligand. The observed Raman bands are in excellent agreement with the single-crystal X-ray diffraction results, confirming the coordination of the Br_2-BDC ligand through its carboxylate oxygen atoms, the 2-MeIm ligands through their nitrogen atoms, and the DMF molecule through its carbonyl oxygen atom to the Cd(II) centre [27]. The combined vibrational and crystallographic analyses therefore provide strong evidence for the successful formation of the one-dimensional coordination polymer.

3.5. SEM–EDS Analysis

The morphology and elemental composition of $[Cd(Br_2\text{-BDC})(2\text{-MeIm})_2(DMF)]_n$ were investigated by scanning electron microscopy (SEM) coupled with energy-dispersive X-ray spectroscopy (EDS) (Fig. S6). The SEM micrographs reveal the formation of well-developed crystalline particles with a predominantly plate-like morphology. The crystals exhibit distinct crystal faces, sharp edges, and relatively smooth surfaces, indicating a high degree of crystallinity and ordered crystal growth. At higher magnification, layered surface features and growth-related textures can be observed on the crystal faces, reflecting the anisotropic growth behaviour of the coordination polymer. The particles are present as aggregated crystalline domains composed of irregularly stacked plate-like crystallites. Minor surface defects and fractured edges are observed on some particles, which are likely associated with crystal cleavage during sample preparation. Nevertheless, the crystals maintain a well-defined morphology and show no evidence of significant amorphous impurities, consistent with the high crystallinity revealed by single-crystal X-ray diffraction analysis. The EDS spectrum confirms the presence of Cd, Br, O, N, and C as the major constituent elements of the material [28]. Strong signals corresponding to cadmium and bromine are clearly observed, while the peaks associated with carbon, nitrogen, and oxygen [29] originate from the Br_2-BDC, 2-MeIm, and DMF ligands. No additional peaks attributable to impurity elements are detected, indicating the high purity of the synthesized coordination polymer. Quantitative EDS analysis yielded elemental contents of 39.03 wt% C, 11.79 wt% N, 19.16 wt% O, 6.99 wt% Br, and 23.03 wt% Cd. These values are consistent with the composition of the cadmium-dibromoterephthalate coordination framework and confirm the successful incorporation of Cd(II) ions, Br_2-BDC, 2-MeIm molecules, and coordinated DMF into the crystalline structure.

3.6. Thermal Analysis

The thermal behaviour of $[Cd(Br_2\text{-BDC})(2\text{-MeIm})_2(DMF)]_n$ was investigated by simultaneous thermogravimetric and differential thermal analysis (TG-DTA) (Fig. S7). The thermogram reveals a multistep decomposition process extending from room temperature to approximately 780°C, indicating the successive removal of coordinated ligands followed by the gradual decomposition of the coordination framework. The first weight-loss stage, completed at 182.46°C, corresponds to a mass loss of 12.12% and is accompanied by an endothermic peak centred at 163.23°C. This process is attributed to the release and decomposition of coordinated DMF molecules together with the initial degradation of the organic ligands. The relatively small mass loss in this temperature range indicates that the

coordination framework remains largely intact during the early stages of heating. The second decomposition stage extends from 187.07 to 334.71°C, exhibiting an additional weight loss of 24.20%. A corresponding endothermic peak is observed at 296.47°C. This stage is associated with the substantial decomposition of the coordinated 2-MeIm ligands and the onset of framework degradation. The disruption of Cd–N and Cd–O coordination bonds contributes significantly to the observed mass loss. The third and major decomposition stage occurs between 337.54 and 682.05°C, resulting in a further weight loss of 51.82%. An endothermic event centred at 360.50°C accompanies this process and corresponds to the decomposition of the dibromoterephthalate (Br_2-BDC) ligands together with the progressive collapse of the remaining coordination network. The large mass loss observed in this region reflects the destruction of the organic backbone and the removal of the majority of carbon-containing species. Beyond approximately 680°C, the thermogram approaches a stable plateau, indicating the completion of the decomposition process and the formation of thermally stable inorganic residues. The remaining residue is attributed to cadmium-containing inorganic species, most likely CdO, formed after complete decomposition of the organic ligands.

3.7. Dielectric studies

The dielectric properties of $[Cd(Br_2\text{-BDC})(2\text{-MeIm})_2(DMF)]_n$ were investigated as functions of frequency and temperature to evaluate the polarization behaviour and dielectric stability of the coordination polymer. The variations of the dielectric constant (ε') and dielectric loss (tan δ) with frequency and temperature are presented in Figs. 6 and 7, respectively. The dielectric response exhibits a pronounced dependence on both frequency and temperature, indicating the contribution of multiple polarization mechanisms within the cadmium-based coordination framework.

The frequency dependence of the dielectric constant (Fig. 6(a)) shows relatively high ε' values in the low-frequency region, followed by a gradual decrease with increasing frequency over the investigated temperature range (40–120°C). The highest dielectric constant is observed at 120°C, where ε' decreases from approximately 14.9 at 100 Hz to about 6.9 at 8 MHz. Similar behaviour is observed at the other temperatures. Such dielectric dispersion is characteristic of polar dielectric materials and arises from the combined contributions of space-charge, dipolar, ionic, and interfacial polarization mechanisms. At low frequencies, the slowly varying electric field provides sufficient time for dipoles and localized charge carriers to align with the applied field, resulting in enhanced polarization and higher dielectric constant values. As the frequency increases, these polarization centres are progressively unable to follow the rapidly alternating electric field, leading to a continuous reduction in polarization and consequently lower ε' values. Above approximately 10^6 Hz, the dielectric constant becomes nearly frequency independent with values close to 6–7, indicating that the slower polarization mechanisms are suppressed, while the dielectric response is governed predominantly by the faster electronic and atomic polarizations [30, 31].

The temperature-dependent dielectric constant (Fig. 7(a)) further demonstrates the thermally activated nature of the polarization processes. At lower frequencies (100 Hz–1 kHz), ε' increases steadily with increasing temperature and reaches its maximum value at 120°C. For example, at 100 Hz, ε' increases

from approximately 10.4 at 40°C to nearly 14.9 at 120°C. This behaviour can be attributed to enhanced dipolar orientation and increased mobility of localized charge carriers at elevated temperatures, which facilitate polarization within the coordination framework. In contrast, only minor changes in ε' are observed above 1 MHz, indicating that the rapid oscillation of the electric field limits the response of thermally activated polarization mechanisms.

The dielectric loss exhibits a frequency dependence similar to that of the dielectric constant (Fig. 6(b)). Relatively high tan δ values are observed at low frequencies, followed by a gradual decrease with increasing frequency, reaching minimum values near 10^6 Hz. A slight increase in dielectric loss is evident at the highest frequencies, particularly at elevated temperatures. The larger dielectric loss in the low-frequency region is attributed to space-charge accumulation, interfacial polarization, and charge-carrier migration, which contribute to energy dissipation within the coordination framework. The absence of a distinct relaxation peak throughout the measured frequency range suggests that the polarization processes are broadly distributed rather than arising from a single well-defined dielectric relaxation mechanism.

The temperature dependence of the dielectric loss (Fig. 7(b)) provides additional insight into the dielectric stability of the coordination polymer. At lower frequencies, tan δ generally increases with increasing temperature owing to enhanced polarization and conduction losses associated with thermally activated charge carriers. In contrast, the dielectric loss remains comparatively low at intermediate and high frequencies and exhibits only a weak temperature dependence. A shallow minimum is observed between 80 and 100°C for several frequencies, followed by a gradual increase at higher temperatures, which may be attributed to the competition between thermally activated charge transport and polarization relaxation. The absence of any pronounced dielectric anomaly or sharp loss maximum throughout the investigated temperature range indicates that no dielectric phase transition occurs between 40 and 120°C [32, 33].

The dielectric behaviour is intrinsically related to the crystal structure of the coordination polymer. The rigid one-dimensional framework, composed of seven-coordinate CdN_2O_5 centres bridged by μ_2-Br_2-BDC ligands and completed by terminal 2-methylimidazole and coordinated DMF molecules, effectively suppresses long-range charge migration while maintaining sufficient dipolar polarization. In addition, intermolecular N–H···O and C–H···O hydrogen-bonding interactions further reinforce the crystal lattice, restricting large-scale dipolar motion and contributing to dielectric stabilization. The observed decrease in both ε' and tan δ with increasing frequency, together with the enhancement of the dielectric response at elevated temperatures, indicates that polarization is thermally activated within the coordination framework [34]. The low-frequency dielectric response is dominated by Maxwell–Wagner interfacial polarization and space-charge effects, whereas electronic and atomic polarization become the principal contributors at higher frequencies. The relatively low dielectric loss maintained in the high-frequency region demonstrates the good dielectric stability of the coordination polymer over the investigated temperature range, suggesting that $[Cd(Br_2\text{-BDC})(2\text{-MeIm})_2(DMF)]_n$ is a promising dielectric material for frequency-dependent electronic applications.

3.8. A.C. conductivity study

The alternating current (A.C.) electrical conductivity behaviour of $[Cd(Br_2\text{-}BDC)(2\text{-}MeIm)_2(DMF)]_n$ was investigated as a function of frequency and temperature in order to understand the charge-transport mechanism operating within the coordination framework. The variations of A.C. conductivity (σ_{ac}) with angular frequency and temperature are presented in Fig. 8(a,b). The conductivity values exhibit a pronounced dependence on both frequency and temperature, indicating the involvement of thermally activated charge-transport processes within the cadmium-based coordination polymer.

The frequency-dependent A.C. conductivity plots (Fig. 8(a)) reveal that the conductivity remains nearly constant and very low in the low-frequency region, followed by a gradual increase with increasing angular frequency for all investigated temperatures. At lower frequencies, the conductivity values are extremely small owing to the limited mobility of charge carriers and the dominance of interfacial polarization effects. As the angular frequency increases, σ_{ac} gradually rises and subsequently increases sharply in the high-frequency region, particularly above $\log\omega \approx 7.0$. Such behaviour is characteristic of hopping-type conduction mechanisms commonly observed in coordination polymers and disordered dielectric materials. The increase in conductivity at higher frequencies can be attributed to enhanced hopping of localized charge carriers between neighbouring coordination sites and increased mobility of polarizable species within the framework.

Among the investigated temperatures, the highest conductivity values are observed at 120 ^{o}C in the high-frequency region, where σ_{ac} reaches approximately 5×10^{-4} S·m^{-1}. The conductivity curves display a systematic increase with frequency, indicating that charge carriers become progressively activated under rapidly oscillating electric fields [35, 36]. The strong frequency dependence suggests that short-range translational hopping of charge carriers dominates the conduction process rather than long-range band-type electronic transport. The polymeric arrangement formed by Cd(II) centres interconnected through Br_2-BDC ligands provides localized pathways that facilitate charge hopping within the coordination network.

The temperature-dependent A.C. conductivity plots measured at different frequencies further support the thermally activated conduction mechanism (Fig. 8(b)). At lower frequencies (100 Hz-100 kHz), the conductivity values remain extremely small throughout the investigated temperature range, indicating restricted charge transport under slowly alternating electric fields. In contrast, higher frequencies such as 3 MHz, 6 MHz, and 8 MHz exhibit significantly larger conductivity values, demonstrating enhanced charge-carrier mobility under rapid field oscillations. At high frequencies, the conductivity exhibits an overall increasing trend with temperature, despite a slight decrease around 80°C, and reaches its maximum values at 120°C. For example, at 8 MHz, the conductivity increases from approximately 2.0 x 10^{-4} S·m^{-1} at 40°C to about 5.0 x 10^{-4} S·m^{-1} at 120°C. A similar but less pronounced behaviour is observed at 6 MHz and 3 MHz. This behaviour may be attributed to thermally activated hopping

processes, increased mobility of localized charge carriers, and enhanced polarization within the coordination framework.

The observed conductivity behaviour may also correlate with the material's dielectric properties. The increase in conductivity at higher frequencies corresponds to the frequency region where dielectric dispersion becomes less pronounced and dielectric loss approaches relatively stable values, suggesting improved charge-transport efficiency under rapidly alternating electric fields. Furthermore, the gradual increase in conductivity with temperature is consistent with the increase in dielectric constant observed at lower frequencies, indicating the participation of thermally activated polarization and charge-carrying species within the framework [37, 38].

Structurally, the seven-coordinate CdN_2O_5 environment formed by Br_2-BDC ligands, coordinated 2-methylimidazole molecules, and DMF ligands plays an important role in governing the electrical transport behaviour. The rigid coordination framework restricts long-range electron delocalization, while localized charge-carrier hopping through intermolecular pathways contributes to the observed A.C. conductivity response. Furthermore, hydrogen-bonding interactions and other weak intermolecular contacts identified from the crystal structure and Hirshfeld surface analysis may influence localized polarization and hopping conduction processes. These intermolecular interactions contribute to framework stabilization while simultaneously providing favourable conditions for short-range charge transport.

The A.C. conductivity studies demonstrate that [Cd(Br_2-BDC)(2-MeIm)$_2$(DMF)] exhibits frequency-dependent hopping conduction with relatively low conductivity values and good electrical stability over the investigated temperature range. The absence of abrupt conductivity anomalies throughout the investigated temperature range suggests that no significant structural or electrical phase transition occurs between 40 and 120°C. The synthesized coordination polymer exhibits predominantly dielectric behaviour, together with thermally activated AC conduction and controlled charge-transport characteristics.

4. Conclusions

A new one-dimensional cadmium(II) coordination polymer, [Cd(Br_2-BDC)(2-MeIm)$_2$(DMF)], was successfully synthesized under solvothermal conditions and comprehensively characterized by single-crystal X-ray diffraction, FT–IR and Raman spectroscopy, Hirshfeld surface analysis, SEM–EDS, thermal analysis, dielectric measurements, and AC conductivity studies. Single-crystal X-ray diffraction revealed that the compound crystallizes in the monoclinic space group $P2_1/n$, where seven-coordinate Cd(II) centres are interconnected by μ_2-2,5-dibromobenzene-1,4-dicarboxylate ligands to generate an infinite one-dimensional coordination polymer. Polyhedral distortion and continuous shape-measure analyses established that the CdN_2O_5 coordination environment adopts a distorted pentagonal-bipyramidal geometry. The crystal structure is further stabilized by intermolecular N–H···O and C–H···O hydrogen-bonding interactions, while Hirshfeld surface analysis demonstrated that H···H, C···H/H···C, O···H/H···O,

and Br···H/H···Br contacts are the dominant contributors to the crystal packing. The spectroscopic results confirmed the coordination of the Br_2-BDC, 2-methylimidazole, and DMF ligands to the Cd(II) centres, in agreement with the crystallographic structure. SEM images revealed well-defined plate-like crystals with good crystallinity, and EDS analysis verified the expected elemental composition of the coordination polymer. Thermal analysis indicated multistep decomposition behaviour and demonstrated that the framework remains thermally stable up to approximately 180°C before the onset of significant ligand decomposition. Dielectric measurements revealed a typical polar dielectric response characterized by a gradual decrease in both the dielectric constant and dielectric loss with increasing frequency and an enhancement of the dielectric response at elevated temperatures. The observed behaviour is attributed to the combined contributions of space-charge, Maxwell–Wagner interfacial, dipolar, and ionic polarization mechanisms. AC conductivity exhibited pronounced frequency and temperature dependence, consistent with a thermally activated hopping-type charge-transport mechanism. The relatively low dielectric loss at high frequencies and the moderate electrical conductivity indicate good dielectric stability while preserving controlled charge transport within the coordination framework. The combined structural and physicochemical investigations establish a clear relationship between the one-dimensional coordination architecture and the dielectric and electrical properties of [Cd(Br_2-BDC)(2-MeIm)$_2$(DMF)]. The rigid Cd(II)-Br_2-BDC framework, reinforced by terminal 2-methylimidazole and coordinated DMF ligands together with intermolecular hydrogen-bonding interactions, provides structural stability while facilitating thermally activated polarization and charge transport. These findings expand the family of brominated Cd(II)-based coordination polymers and demonstrate their potential as dielectric materials for frequency-dependent electronic applications.

Declarations

Author Contribution

B.C.T. performed the synthesis of the material and contributed to Writing – original draft. Y.Y.Y. contributed to Conceptualization, Investigation, and Data curation. K.K.T. contributed to Conceptualization, Investigation, and Data curation. A.K.T. contributed to Conceptualization, Investigation, and Data curation. A.A.P. contributed to Writing – original draft and Writing – review & editing. A.K.R. contributed to Conceptualization, Investigation, and Data curation. A.S.N. contributed to Conceptualization, Investigation, and Data curation. A.B.I. contributed to Conceptualization, Investigation, and Data curation. L.B. contributed to Conceptualization, Investigation, and Data curation. S.E. contributed to Conceptualization, Investigation, and Data curation. A.B.I. contributed to Conceptualization, Investigation, and Data curation. C.B. contributed to Writing – original draft and Writing – review & editing. All authors reviewed and approved the final manuscript.

Supplementary materials

CCDC 2564892 contains the supplementary crystallographic data for this paper. These data can be obtained free of charge from The Cambridge Crystallographic Data Centre *via* www.

ccdc.cam.ac.uk/data request/cif.

Acknowledgements

The authors thank the Institute of General and Inorganic Chemistry of the Uzbekistan Academy of Sciences for providing instrumental support facilities throughout the research.

The authors would like to thank the "**Centre of Collective Usage**" at the Institute of Bioorganic Chemistry named after A. Sadikov of the Academy of Sciences of the Republic of Uzbekistan for their instrumental support of the research.

Data availability statement

The data used to support the findings of the study are available from the corresponding author upon request.

Funding

The authors gratefully acknowledge the support of the Academy of Sciences of the Republic of Uzbekistan. The work was carried out by the "**Nano and Composition Materials**" laboratory at the Institute of General and Inorganic Chemistry.

Declaration of competing interest

The authors declare that they have no known competing financial interests or personal relationships that could have appeared to influence the work reported in this paper.

Ethical approval

Not Applicable.

References

1. X.W. Wang, L. Fu, G.H. Cui, Three robust Zn (□)-coordination polymers as dual-responsive chemosensors for efficient sensing of enrofloxacin and acetylacetone. J. Mol. Struct. **1289**, 135881 (2023). https://doi.org/10.1016/j.molstruc.2023.135881
2. Y. Sun, Y. Sun, H. Zheng, H. Wang, Y. Han, Y. Yang, L. Wang, Four calcium (II) coordination polymers based on 2, 5-dibromoterephthalic acid and different N-donor organic species: Syntheses, structures, topologies, and luminescence properties. CrystEngComm. **18**(44), 8664–8671 (2016). https://doi.org/10.1039/C6CE01709F
3. M. Parsaei, K. Akhbari, S. Kawata, Computational Simulation of CO2/CH4 Separation on a Three-Dimensional Cd-Based Metal–Organic Framework. Cryst. Growth. Des. **23**(8), 5705–5718 (2023). https://doi.org/10.1021/acs.cgd.3c00366

4. M. Parsaei, K. Akhbari, E. Tylianakis, G.E. Froudakis, J.M. White, S. Kawata, Computational study of two three-dimensional Co (II)-based metal–organic frameworks as quercetin anticancer drug carriers. Cryst. Growth. Des. **22**(12), 7221–7233 (2022). https://doi.org/10.1021/acs.cgd.2c00900
5. S. Liu, Q. Dong, D. Wang, Y. Wang, H. Wang, Y. Huang, S. Wang, L. Liu, J. Duan, Interplay of tri-and bidentate linkers to evolve micropore environment in a family of quasi-3D and 3D porous coordination polymers for highly selective CO2 capture. Inorg. Chem. **58**(23), 16241–16249 (2019). https://doi.org/10.1021/acs.inorgchem.9b02774
6. X. Zhang, Y. Zhang, S. Jiao, X. Song, S. Li, K. Liu, L. Wang, Coordination polymers driven by 2, 5-dibromoterephthalic acid and chelating co-ligands: Syntheses, structures and luminescent properties. J. Solid State Chem. **292**, 121721 (2020). https://doi.org/10.1016/j.jssc.2020.121721
7. W. Liu, F. Wang, X. Chen, W. Zhi, X. Wang, B. Xu, B. Yang, Design of turn-off luminescent Ln-MOFs for sensitive detection of cyanide anions. Dalton Trans. **51**(41), 15741–15749 (2022). https://doi.org/10.1039/D2DT01844F
8. Y. Sun, Y. Sun, H. Zheng, H. Wang, Y. Han, Y. Yang, L. Wang, Four calcium (II) coordination polymers based on 2, 5-dibromoterephthalic acid and different N-donor organic species: Syntheses, structures, topologies, and luminescence properties. CrystEngComm. **18**(44), 8664–8671 (2016). https://doi.org/10.1039/C6CE01709F
9. S. Zhang, L. Chen, J. Xie, Y. Zhang, F. Huang, X. Wang, K. Li, F. Zhai, Q. Yang, L. Chen, Y. Wang, Turn-up luminescent sensing of ultraviolet radiation by lanthanide metal–organic frameworks. Inorg. Chem. **61**(11), 4561–4565 (2022). https://doi.org/10.1021/acs.inorgchem.2c00250
10. S. Zhang, Y. Yang, Z.Q. Xia, X.Y. Liu, Q. Yang, Q. Wei, G. Xie, S.P. Chen, S.L. Gao, Eu-MOFs with 2-(4-carboxyphenyl) imidazo [4, 5-f]-1, 10-phenanthroline and ditopic carboxylates as coligands: synthesis, structure, high thermostability, and luminescence properties. Inorg. Chem. **53**(20), 10952–10963 (2014). https://doi.org/10.1021/ic501253c
11. C.A. O'Keefe, C. Mottillo, J. Vainauskas, L. Fabian, T. Friscic, R.W. Schurko, NMR-enhanced crystallography aids open metal–organic framework discovery using solvent-free accelerated aging. Chem. Mater. **32**(10), 4273–4281 (2020). https://doi.org/10.1021/acs.chemmater.0c00894
12. Y.X. Sun, W.Y. Sun, Zinc (II)–and cadmium (II)–organic frameworks with 1-imidazole-containing and 1-imidazole-carboxylate ligands. CrystEngComm. **17**(22), 4045–4063 (2015). https://doi.org/10.1039/C5CE00372E
13. F. Semerci, O.Z. Yeşilel, M.S. Soylu, S. Keskin, O. Büyükgüngör, A two-dimensional photoluminescent cadmium (II) coordination polymer containing a new coordination mode of pyridine-2, 3-dicarboxylate: Synthesis, structure and molecular simulations for gas storage and separation applications. Polyhedron. **50**(1), 314–320 (2013). https://doi.org/10.1016/j.poly.2012.10.009
14. G.S. Kürkçüoğlu, O.Z. Yeşilel, İ. Çaylı, O. Büyükgüngör, One-and two-dimensional cadmium (II) tetracyanonickelate (II) coordination polymers with imidazole and 2-methylimidazole ligands. J. Inorg. Organomet. Polym Mater. **21**(2), 306–315 (2011). https://doi.org/10.1007/s10904-010-9454-6

15. G. Günay, O.Z. Yeşilel, C. Darcan, S. Keskin, O. Büyükgüngör, Synthesis, crystal structures, molecular simulations for hydrogen gas adsorption, fluorescent and antimicrobial properties of pyrazine-2, 3-dicarboxylate complexes. Inorg. Chim. Acta. **399**, 19–35 (2013). https://doi.org/10.1016/j.ica.2012.12.036
16. X. Li, X. Sun, X. Li, Z. Fu, Y. Su, G. Xu, Porous cadmium (II) anionic metal–organic frameworks based on aromatic tricarboxylate ligands: Encapsulation of protonated flexible bis (2-methylimidazolyl) ligands and proton conductivity. Cryst. Growth. Des. **15**(9), 4543–4548 (2015). https://doi.org/10.1021/acs.cgd.5b00799
17. J. Wang, J.H. Yu, Q.F. Yang, J.Q. Xu, New Thiocyanatocadmate and Halo-thiocyanatocadmates Modified by Imidazole or Triazole Derivatives: Synthesis, Structural Characterization, and Photoluminescence Property. J. Cluster Sci. **29**(3), 499–508 (2018). https://doi.org/10.1007/s10876-018-1358-6
18. D.K. ugli Saidov, K.K. Turaev, A. Kumar, S.A. Kasimov, B.Z. Adizov, Y.Y. Yakubov, K.S. Tassibekov, B. Chellakarungu, A.S. Normamatov, M. Ubaidullah, A.M. Al-Enizi, Synthesis, structural characterization, and antimicrobial activity of cadmium (II) coordination polymer derived from 1, 10-phenanthroline and tartaric acid. J. Mol. Struct. 146200 (2026). https://doi.org/10.1016/j.molstruc.2026.146200
19. Z.W. He, C.J. Liu, W.D. Li, S.S. Han, S.S. Chen, Two interpenetrated Zn (II) coordination polymers: synthesis, topological structures, and property. Crystals. **9**(11), 601 (2019). https://doi.org/10.3390/cryst9110601
20. X. Zhang, Y. Zhang, S. Jiao, X. Song, S. Li, K. Liu, L. Wang, Coordination polymers driven by 2, 5-dibromoterephthalic acid and chelating co-ligands: Syntheses, structures and luminescent properties. J. Solid State Chem. **292**, 121721 (2020). https://doi.org/10.1016/j.jssc.2020.121721
21. A.H. Bakheit, H.A. Abuelizz, R. Al-Salahi, Hirshfeld surface analysis and density functional theory calculations of 2-benzyloxy-1, 2, 4-triazolo [1, 5-a] quinazolin-5 (4 H)-one: a comprehensive study on crystal structure, intermolecular interactions, and electronic properties. Crystals. **13**(10), 1410 (2023). https://doi.org/10.3390/cryst13101410
22. M. Bergedahl, P. Narea, J. Llanos, R. Pulido, N. Naveas, P. Amo-Ochoa, F. Zamora, G.E. Delgado, F.M. Galleguillos Madrid, Y. León, I. Brito, Synthesis, Crystal Structures, Hirshfeld Surface Analysis, Computational Investigations, Thermal Properties, and Electrochemical Analysis of Two New Cu (II) and Co (II) Coordination Polymers with the Ligand 5-Methyl-1-(pyridine-4-yl-methyl)-1H-1, 2, 3-triazole-4-carboxylate. Int. J. Mol. Sci. **26**(4), 1671 (2025). https://doi.org/10.3390/ijms26041671
23. D.L. Reger, A. Debreczeni, M.D. Smith, Zinc paddlewheel dimers containing a strong π··· π stacking supramolecular synthon: designed single-crystal to single-crystal phase changes and gas/solid guest exchange. Inorg. Chem. **50**(22), 11754–11764 (2011). https://doi.org/10.1021/ic201830h
24. C.W. Tsai, R.E. Kroon, H.C. Swart, J.J. Terblans, R.A. Harris, Photoluminescence of metal-imidazolate complexes with Cd (II), Zn (II), Co (II) and Ni (II) cation nodes and 2-methylimidazole organic linker. J. Lumin. **207**, 454–459 (2019). https://doi.org/10.1016/j.jlumin.2018.11.026

25. Di A. Santo, G.A. Echeverría, O.E. Piro, H. Pérez, A.B. Altabef, D.M. Gil, Supramolecular architectures in luminescent Zn (II) and Cd (II) complexes containing imidazole derivatives: Crystal structures, vibrational and thermal properties, Hirshfeld surface analysis and electrostatic potentials. J. Mol. Struct. **1134**, 492–503 (2017). https://doi.org/10.1016/j.molstruc.2017.01.028
26. G. Świderski, A. Jabłońska-Trypuć, M. Kalinowska, R. Świsłocka, D. Karpowicz, M. Magnuszewska, W. Lewandowski, Spectroscopic, theoretical and antioxidant study of 3d-transition metals (Co (II), Ni (II), Cu (II), Zn (II)) complexes with cichoric acid. Materials. **13**(14), 3102 (2020). https://doi.org/10.3390/ma13143102
27. A.Y. Lee, D.Y. Park, M.S. Jeong, Correlational study of halogen tuning effect in hybrid perovskite single crystals with Raman scattering, X-ray diffraction, and absorption spectroscopy. J. Alloys Compd. **738**, 239–245 (2018). https://doi.org/10.1016/j.jallcom.2017.12.149
28. K. Martinello, M.L. Oliveira, F.A. Molossi, C.G. Ramos, E.C. Teixeira, R.M. Kautzmann, L.F. Silva, Direct identification of hazardous elements in ultra-fine and nanominerals from coal fly ash produced during diesel co-firing. Sci. Total Environ. **470**, 444–452 (2014). https://doi.org/10.1016/j.scitotenv.2013.10.007
29. P. Keerthana, A.K. Das, M. Bharath, M. Ghosh, A. Varghese, A ratiometric fluorescent sensor based on dual-emissive carbon dot for the selective detection of Cd2+. J. Environ. Chem. Eng. **11**(2), 109325 (2023). https://doi.org/10.1016/j.jece.2023.109325
30. F. Wu, A. Xie, L. Jiang, S. Mukherjee, H. Gao, J. Shi, J. Wu, H. Shang, Z. Sheng, R. Guo, L. Wu, Inorganic–organic hybrid dielectrics for energy conversion: mechanism, strategy, and applications. Adv. Funct. Mater. **33**(28), 2212861 (2023). https://doi.org/10.1039/D2TC00193D
31. J.W. Zha, M.S. Zheng, B.H. Fan, Z.M. Dang, Polymer-based dielectrics with high permittivity for electric energy storage: A review. Nano Energy. **89**, 106438 (2021). https://doi.org/10.1016/j.nanoen.2021.106438
32. H. Abdelkefi, H. Khemakhem, G. Vélu, J.C. Carru, V. Mühll, R, Dielectric properties and ferroelectric phase transitions in BaxSr1 – xTiO3 solid solution. J. Alloys Compd. **399**(1–2), 1–6 (2005). https://doi.org/10.1016/j.jallcom.2005.03.007
33. J. Suchanicz, M. Nowakowska-Malczyk, A. Kania, A. Budziak, K. Kluczewska-Chmielarz, P. Czaja, D. Sitko, M. Sokolowski, A. Niewiadomski, T.V. Kruzina, Effects of electric field poling on structural, thermal, vibrational, dielectric and ferroelectric properties of Na0. 5Bi0. 5TiO3 single crystals. J. Alloys Compd. **854**, 157227 (2021). https://doi.org/10.1016/j.jallcom.2020.157227
34. B. Luo, X. Wang, Y. Wang, L. Li, Fabrication, characterization, properties and theoretical analysis of ceramic/PVDF composite flexible films with high dielectric constant and low dielectric loss. J. Mater. Chem. A **2**(2), 510–519 (2014). https://doi.org/10.1039/C3TA14107A
35. A. Ghoudi, S. Auguste, J. Lhoste, W. Rekik, H. Ghalla, K. Khirouni, A. Aydi, A. Oueslati, Crystal structure and spectroscopic characterization of a new hybrid compound,(C12H17N2) 2 [CdBr4], for energy storage applications. ACS omega. **9**(26), 28339–28353 (2024). https://doi.org/10.1021/acsomega.4c01997

36. X. Zhi, H. Yu, Q. Liu, Y. Guo, R. Lin, J. Wu, Z. Cao, L. Yang, Engineering High-Performance Dielectric Thin Films from Poly (methyl methacrylate)(PMMA)/Metal–Organic Complex Hybrid. Ind. Eng. Chem. Res. **65**(14), 7605–7618 (2026). https://doi.org/10.1021/acs.iecr.6c00313
37. D. Sivam, B.C. ugli Tursunov, S. Sivakolunthu, R. Duraisamy, G. Loganathan, A.B. Ibragimov, B. Chellakarungu, Enhanced SHG efficiency in a donor–acceptor 4-cyanopyridine· 2, 4-dinitrophenol cocrystal: synthesis, characterization and optical studies. Opt. Mater. 117638 (2025). https://doi.org/10.1016/j.optmat.2025.117638
38. S. Zhang, J. Zheng, Z. Zhao, S. Du, D. Lan, Z. Gao, G. Wu, New prospects in built-in electric fields for electromagnetic wave absorption: from fundamentals to interdisciplinary applications. Adv. Funct. Mater. **36**(1), e13762 (2026). https://doi.org/10.1002/adfm.202513762

Figures

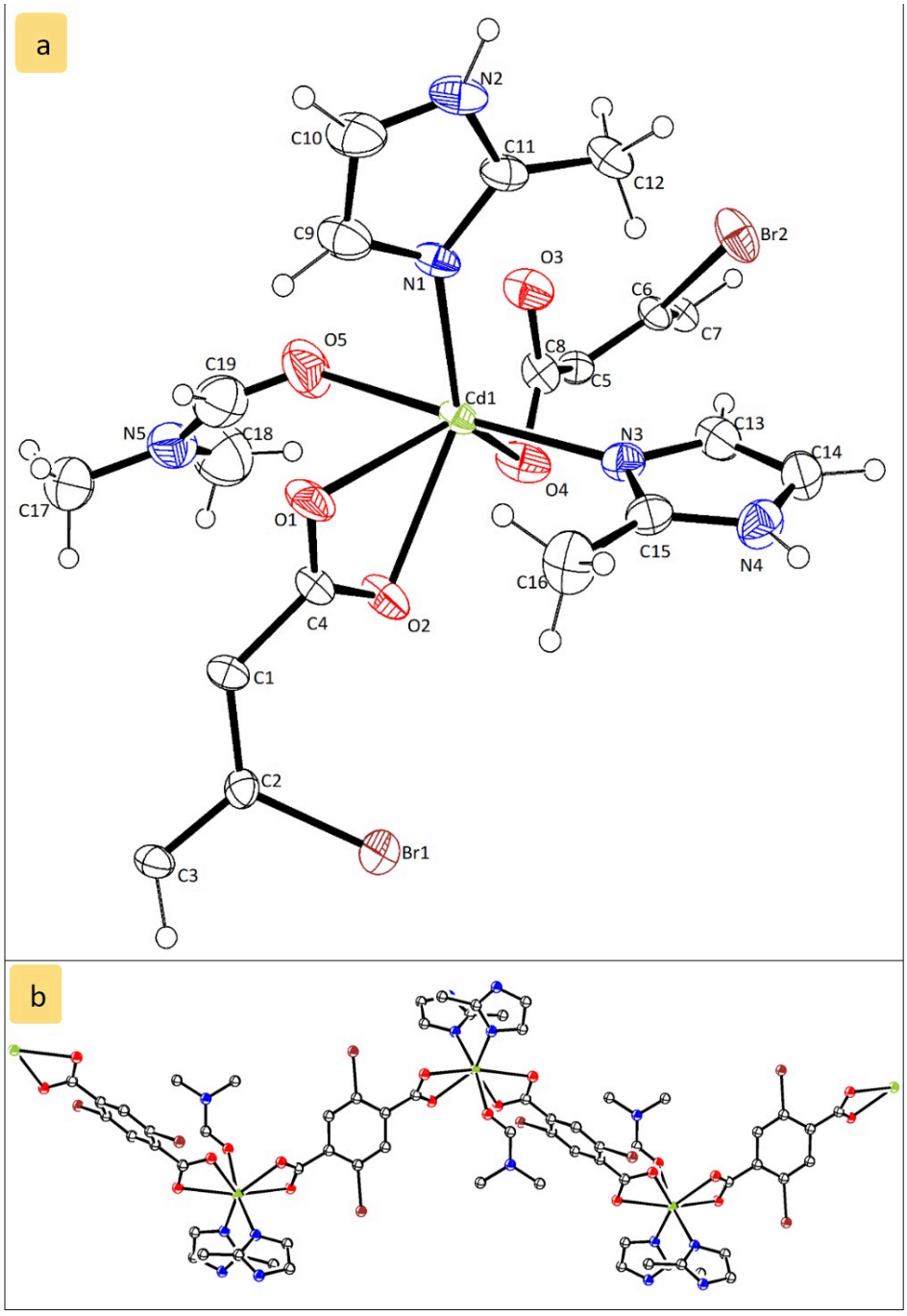


Figure 1

Crystal structure of $[Cd(Br_2\text{-}BDC)(2\text{-}MeIm)_2(DMF)]_n$: (a) ORTEP representation with displacement ellipsoids drawn at the 35% probability level; (b) one-dimensional (1D) coordination polymer chain.

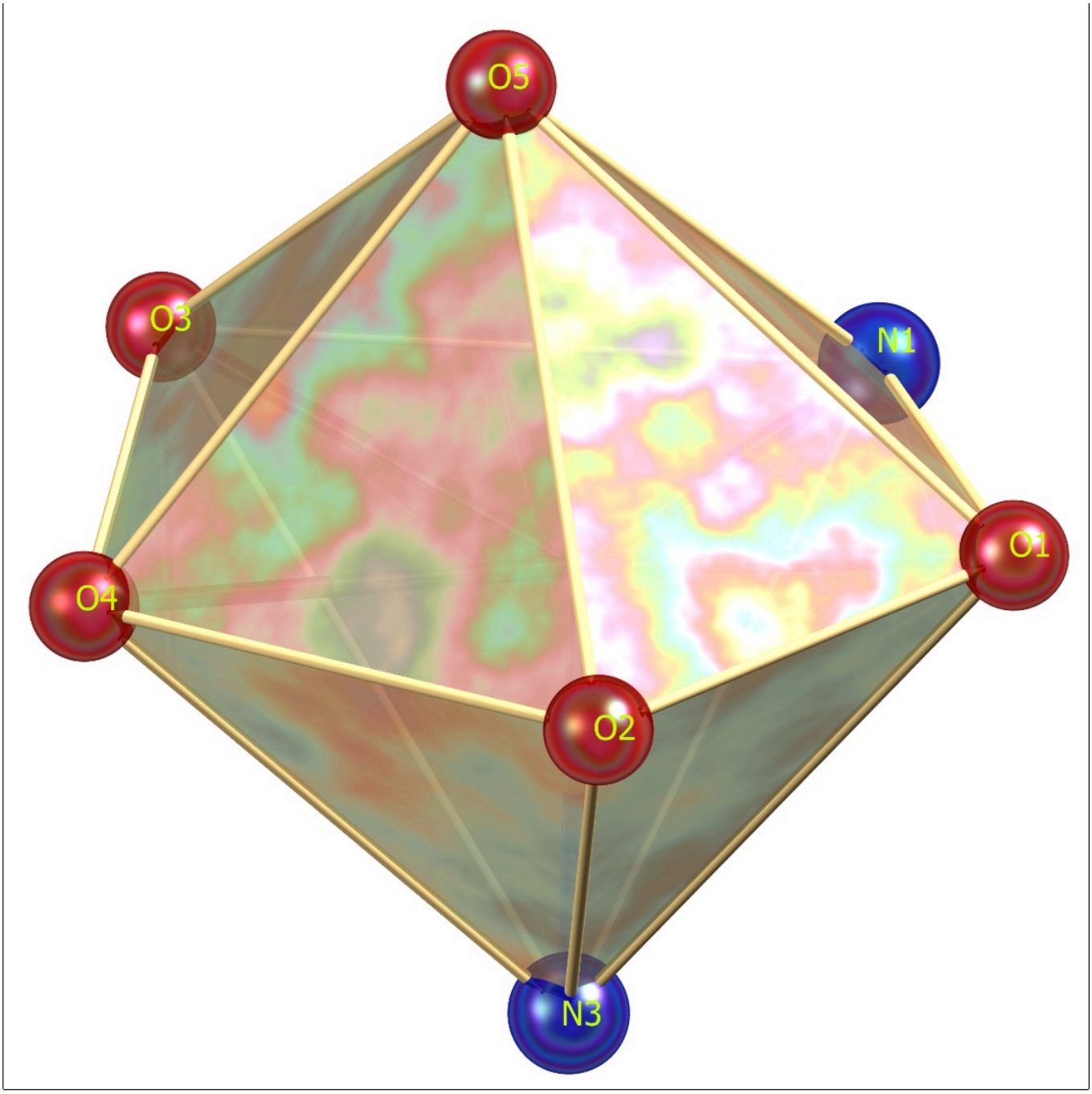


Figure 2

Polyhedral representation of the coordination environment around the Cd(II) metal centre.

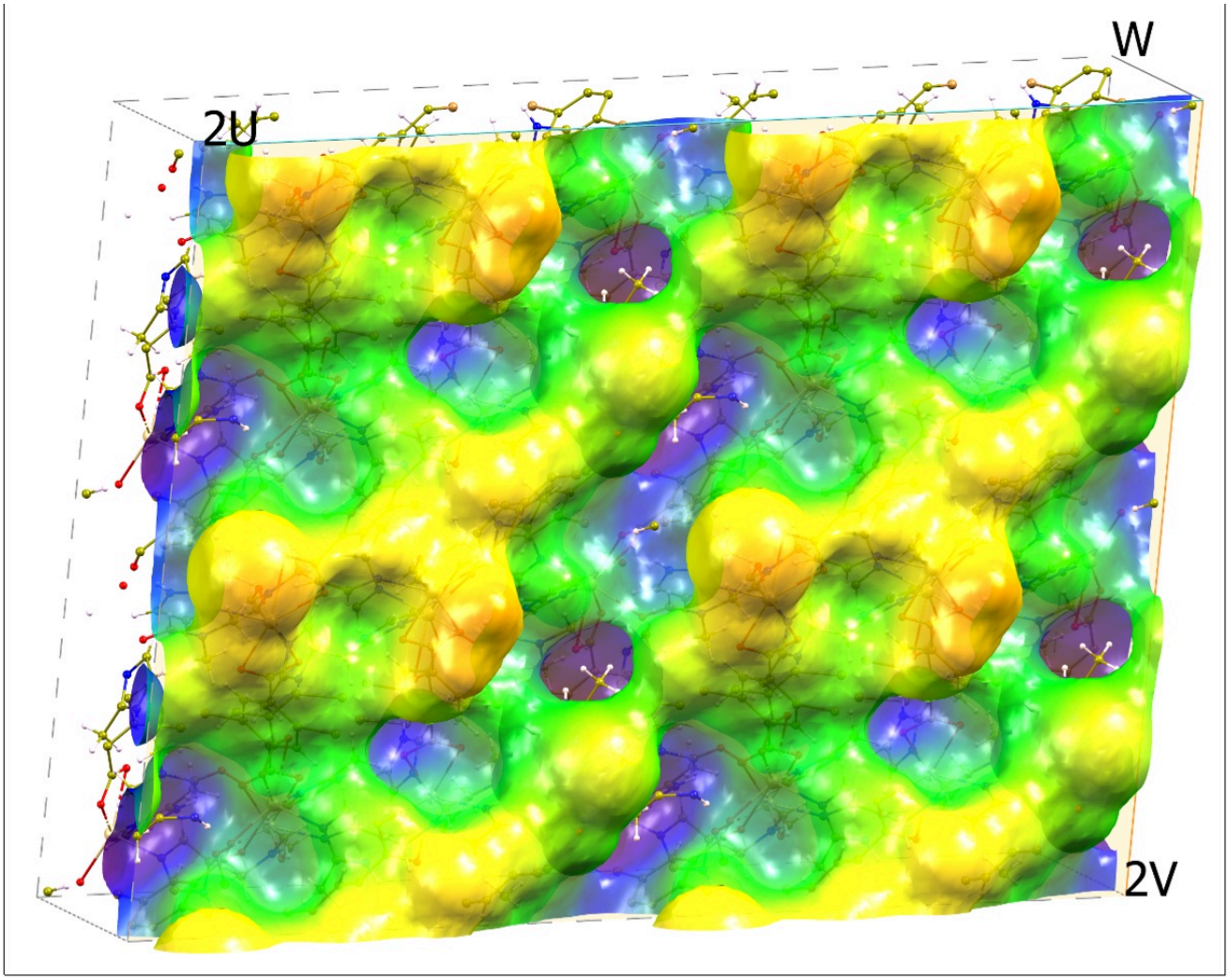


Figure 3

Topology-coloured solvent-accessible surface of $[Cd(Br_2\text{-}BDC)(2\text{-}MeIm)_2(DMF)]_n$ generated using Mercury with a probe radius of 1.2 Å, illustrating the distribution of accessible voids and the crystal packing features.

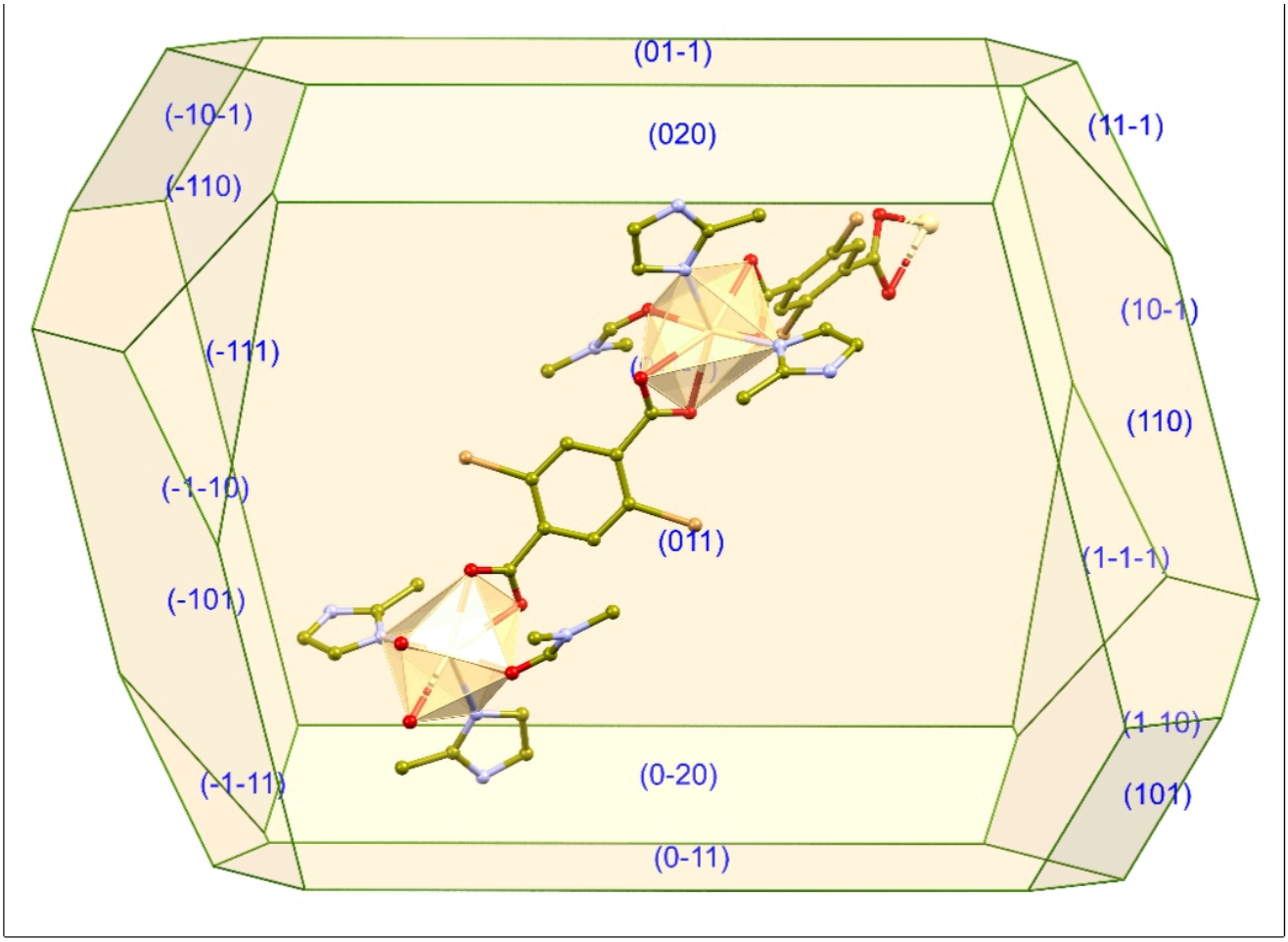


Figure 4

Predicted crystal morphologies with indexed face of $[Cd(Br_2\text{-}BDC)(2\text{-}MeIm)_2(DMF)]_n$.

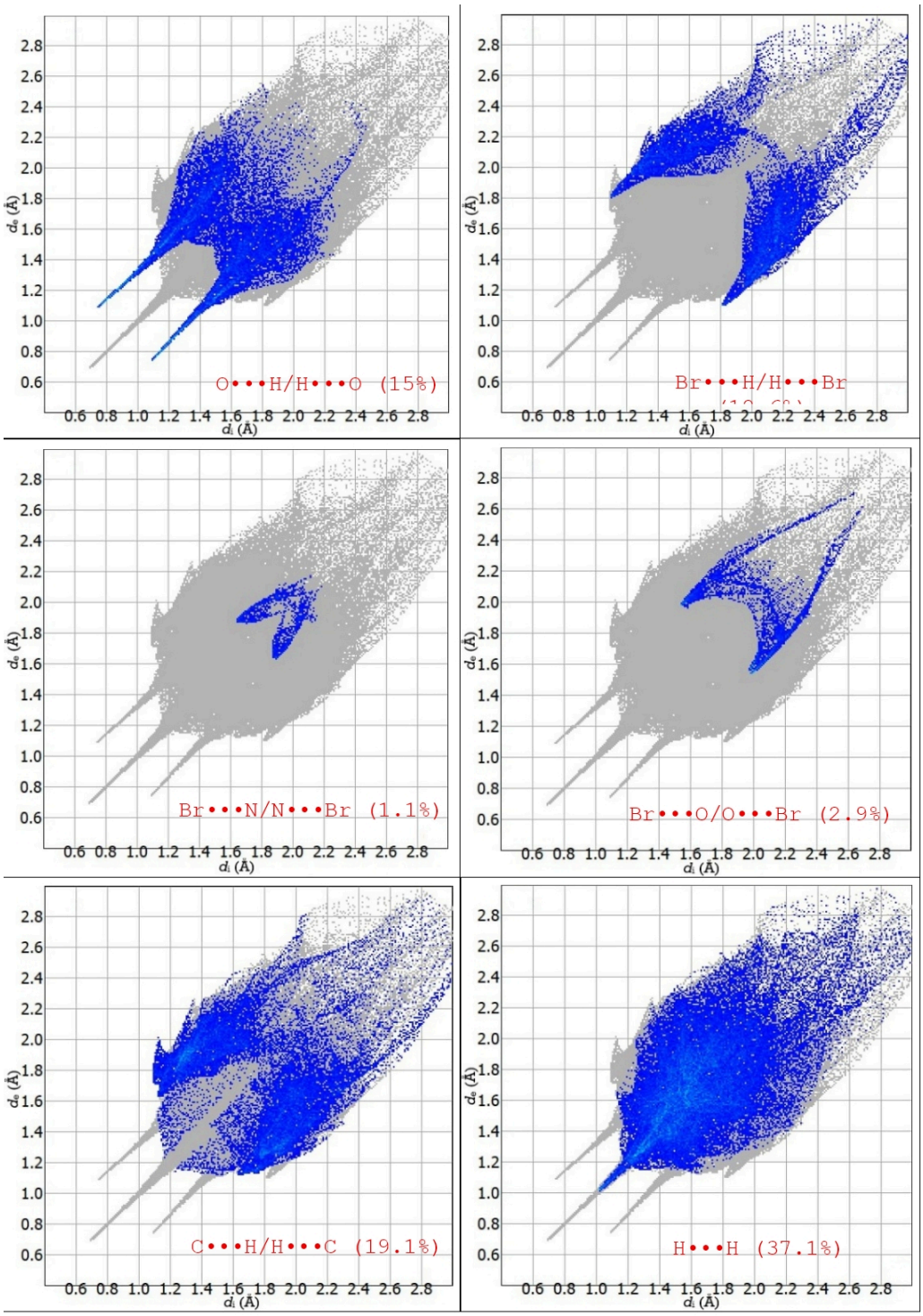


Figure 5

Fingerprint plots of $[Cd(Br_2\text{-}BDC)(2\text{-}MeIm)_2(DMF)]_n$

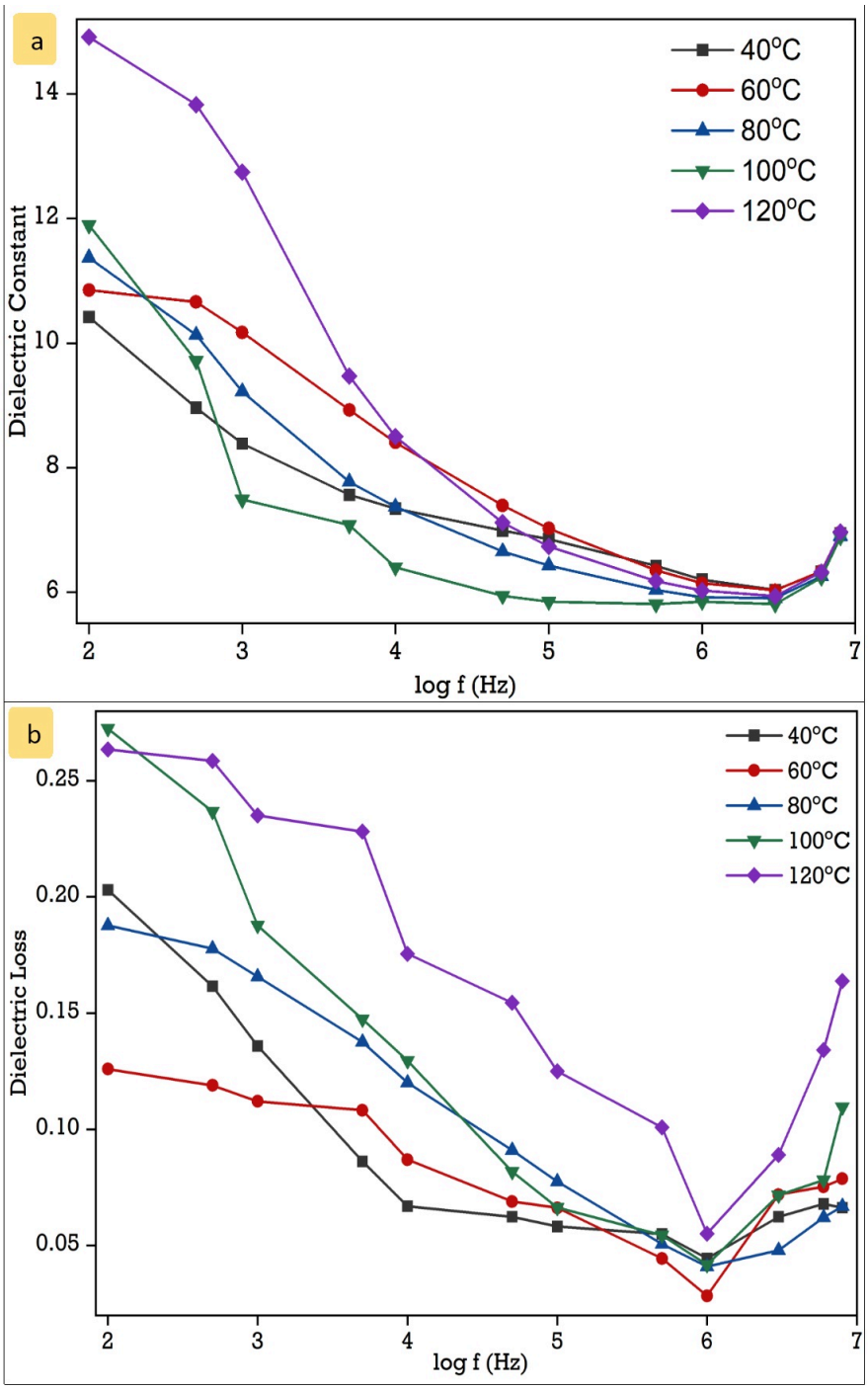


Figure 6

Frequency-dependent dielectric properties of $[Cd(Br_2\text{-}BDC)(2\text{-}MeIm)_2(DMF)]_n$ measured at various temperatures: (a) variation of the dielectric constant with logarithmic frequency (log *f*), and (b) variation of the dielectric loss with log *f*.

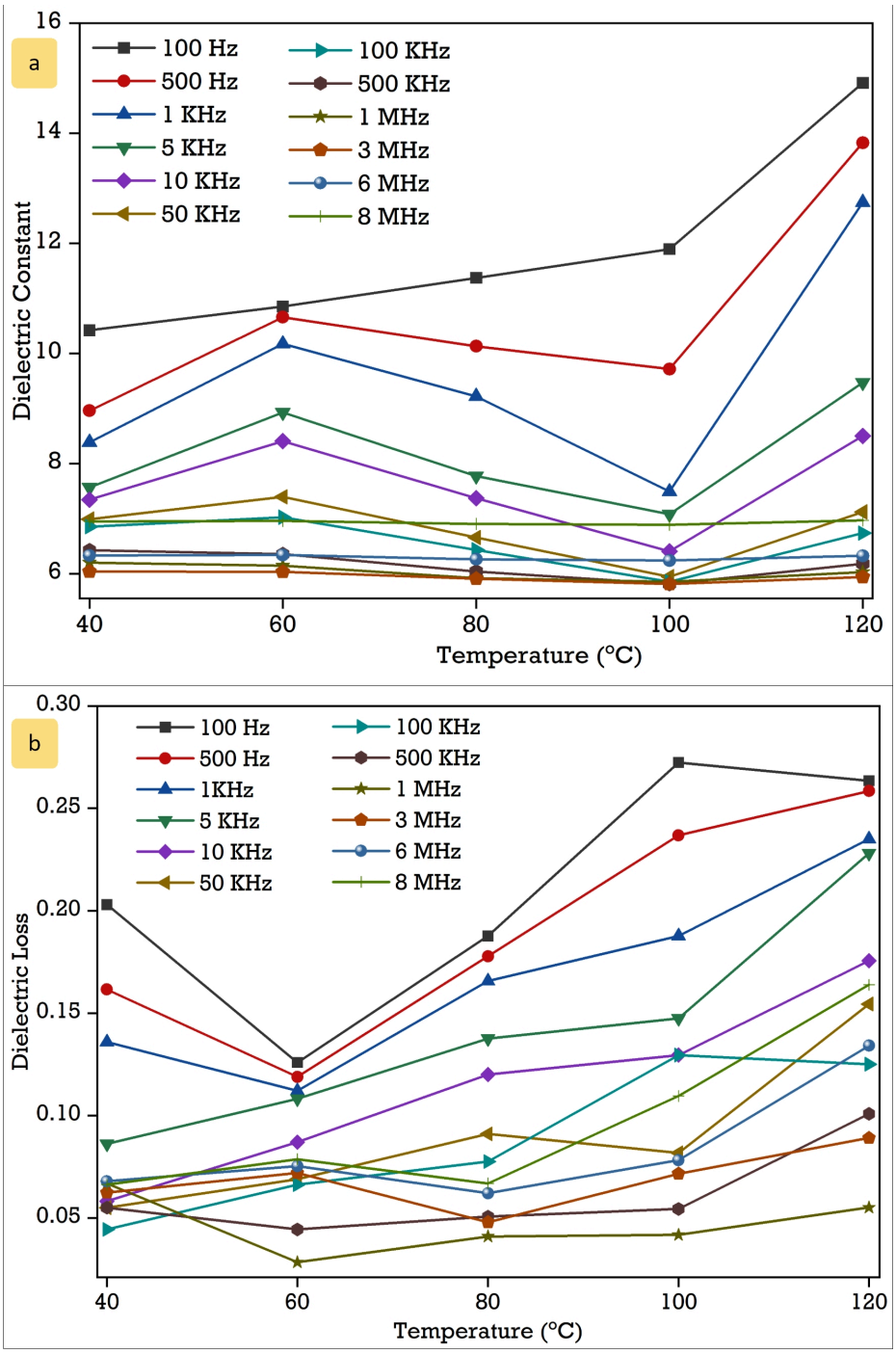


Figure 7

Temperature-dependent dielectric properties of $[Cd(Br_2\text{-}BDC)(2\text{-}MeIm)_2(DMF)]_n$ measured at various frequencies: (a) variation of the dielectric constant with temperature, and (b) variation of the dielectric loss with temperature.

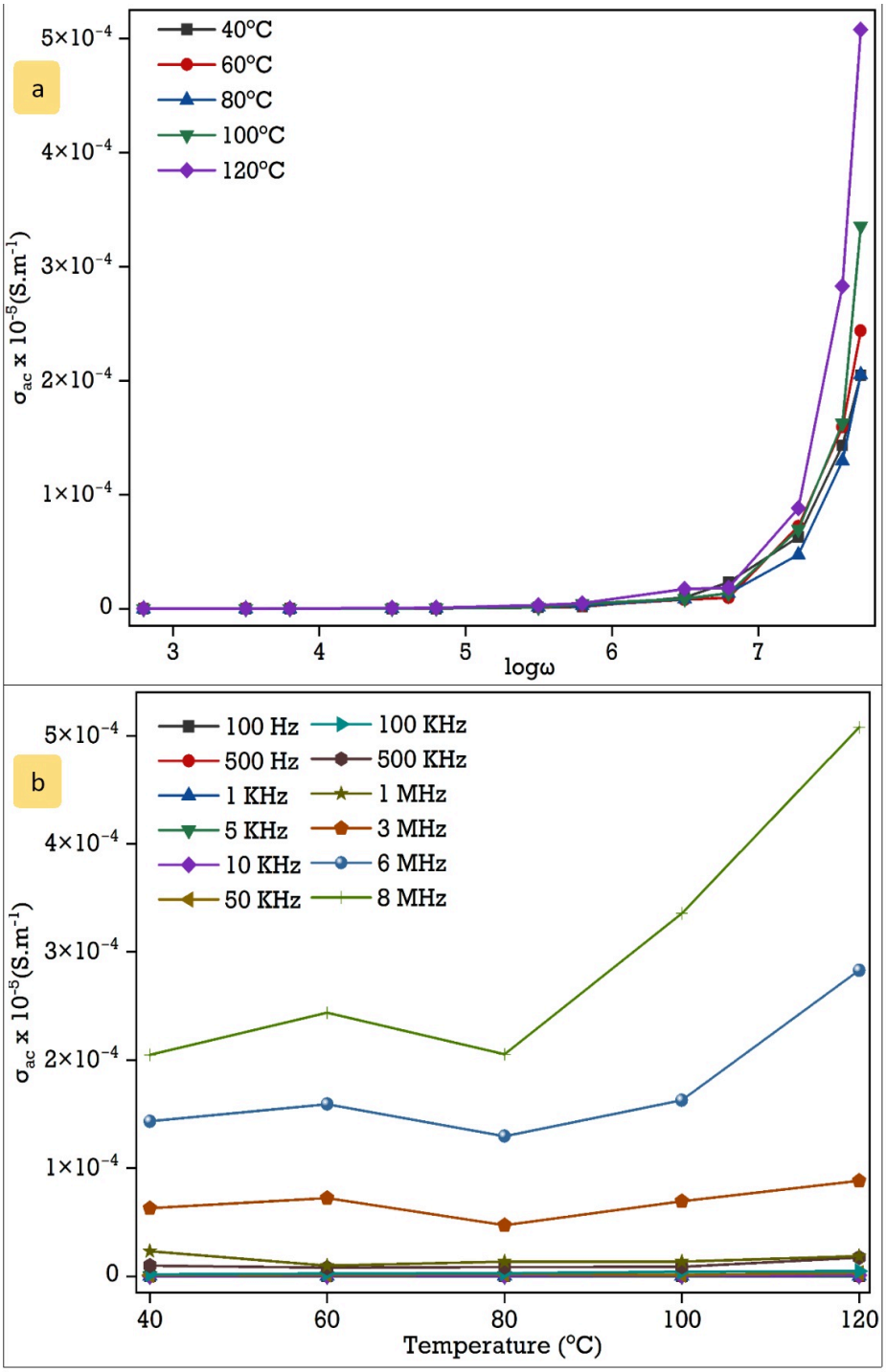


Figure 8

AC conductivity of $[Cd(Br_2\text{-}BDC)(2\text{-}MeIm)_2(DMF)]_n$ measured at various temperatures and frequencies: (a) variation of the AC conductivity with log ω at various temperatures, and (b) variation of the AC conductivity with temperature at various frequencies.

Supplementary Files

This is a list of supplementary files associated with this preprint. Click to download.

- SupportingInformation.docx